BACKPACK SYSTEM FOR CAPTURING 3D POINT CLOUDS OF FORESTS

M. Goebel *, D. Iwaszczuk

Technical University of Darmstadt, Remote Sensing and Images Analysis, Darmstadt, Germany
(mona.goebel, dorota.iwaszczuk)@tu-darmstadt.de

KEY WORDS: SLAM, LiDAR, Multi-Spectral Camera, Mobile Mapping, Terrestrial Laser Scanning, Vegetation

ABSTRACT:

A 3D model can be useful for inventory management and monitoring of forests. For this task, we present our prototype mobile mapping backpack system for collecting 3D point clouds of forest vegetation. However, data collection in forests is challenging due to unreliable GNSS positioning, moving objects caused by winds, unclear object edges, and uneven ground to walk on. We include LiDAR and IMU with Simultaneous Localisation and Mapping (SLAM). We describe in detail our backpack system, its development for the forest environment, and evaluate it. Furthermore, we compare two open code SLAM algorithms for ROS, as well as data collection and laser scan quality between TLS and MLS for forest environments. Finally, we installed and tested the MicaSense multi-spectral camera on our backpack and discuss the advantages and drawbacks of it. We conclude, that the backpack is convenient to use in forest environments and produces a good point cloud. It can be carried easily off trail and on rough terrain. The system needs less storage space, computation and less collection time than TLS.

1. INTRODUCTION

Forest are essential environments as they regulate air and water quality, provide lumber, and preserve biodiversity of flora and fauna. Trees have to deal with water shortages and temperature extremes. Therefore, it is essential to be aware of the state of the forest, which necessitates collecting data repeatedly and keeping it up to date. Forest status are reported annually, for example in Germany, collecting data through visual interpretation and measuring trees (Talkner et al., 2022). Future decisions, such as planting the right tree species or enforcing regulations, depend on information such as vegetation quantity, which can be collected via laser scanning, and forest health, for example derived from multi-spectral images. Digital approaches have shown to improve the quality and quantity of forest information (Bettinger et al., 2023), addressing the slow manual data collection process. Many approaches are being tested including satellite and airborne images as well as LiDAR collected from above or beneath the canopy. In this study, we develop a prototype mobile system for spotlight mapping of forests. We aim at not only capturing the geometry of the scene, but also at mapping the vegetation health.

1.1 Related Work

There are numerous platforms that have been used to attach a laser. Four main groups can be named, with the first being Airborne Laser Scanning (ALS). Terrestrial Laser Scanning (TLS) is the next group, where the scanner is mounted in a fixed position on a tripod and only used in between single scans. The last two are UAV (Unmanned Aerial Aircraft, mostly drones) Laser Scanning (ULS) and Mobile Laser Scanning (MLS). The latter includes all platforms that move on the ground during scanning, such as cars, bicycles, Segways, carts as well as human carried systems like handhelds or backpacks.

Laser Scanning in Forests. Capturing forests was realised to improve forest inventories, long-term monitoring or the forest as biomass and carbon sink (Liang et al., 2016, 2018; Campos et al., 2020; Calders et al., 2022). TLS has also been used to analyse the burn severity in forests (Gallagher et al., 2021). The detection of single trees in a forest is a major goal in common research. Typically, these methods involve data collected from above the canopy with ALS data (Jeronimo et al., 2018; Heinzel and Ginzler, 2019; Stereńczak et al., 2020). Looking through the canopy can be difficult with ALS in different forest tree densities (Zong et al., 2021). Additionally, the TLS registration is more challenging in forest than in urban areas (Pohjavirta et al., 2022). Furthermore, researchers have not only concentrated on trees, but also on the lower forest vegetation (Wallace et al., 2020; Huo et al., 2022; Iwaszczuk et al., 2023). For a laser scanning procedure, one single wavelength is common practice. However, Elsherif et al. (2019) showed that using a dual-wavelength on trees has advantages. When combining near-infrared (808 nnm) and shortwave-infrared (1550 nm), they could calculate the Normalised Difference Index (NDI), as well as estimating the leaf Equivalent Water Thickness (EWT)

Figure 1. Self-built prototype mobile mapping backpack system.

* Corresponding author

and the Fuel Moisture Content (FMC). Kukko et al. (2017) developed a scanning system on an all-terrain vehicles using GNSS antenna, LiDAR, and IMU. They developed a new algorithm for SLAM using graph representation. Shao et al. (2020) combined TLS and MLS for forest mapping, using SLAM to register single MLS scans and improve them based on TLS data. For further reading, we refer the reader to Guo et al. (2021), which highlights the usage of LiDAR in ecological observation, as well as Liang et al. (2022) which addresses remote sensing of forests.

SLAM. Simultaneous Localisation and Mapping (SLAM) has been developed for many years, especially in the robotic field. The task is to create a map while also trying to locate oneself. For instance, a robot is placed into an apartment and it is supposed to generate a floor plan and connecting the individual rooms, while sending its location to the home base. This is what a robotic vacuum cleaner does. In the field of remote sensing, apart from buildings, the SLAM method is used for mapping urban areas such as streets and campuses, as well as parks and forests. One well-known algorithm is LOAM Zhang and Singh (2014), which stands for LiDAR Odometry and Mapping. Successors are for example LeGo-LOAM (Shan et al., 2020) and F-LOAM (Wang et al., 2021). The newest publication is Fast-LIO2 by Xu et al. (2021a). SLAM based on DeepLearning models was also tested, such as DeepLIO (Javanmard-Gh. et al., 2021). A full overview of the different SLAM approaches and development is presented in Xu et al. (2022).

Backpack Systems. Compared to other mobile mapping systems, backpack systems are more flexible. The user is not restricted by stairs, terrain quality, or car-accessible roads. The data collection is quick, and you need only one operator. Lauterbach et al. (2015) developed a backpack system with a heavy Riegl LiDAR for 3D and SICK LiDAR for 2D scanning, a low-cost IMU, and a GNSS antenna. The system compensates carrier movements and aligns single laser scans, with a maximum translation pose error of 25 cm and 7° in rotation. The software is based on ROS and uses the HectorSLAM algorithm (Kohlbrecher et al., 2011). Velas et al. (2019) constructed a backpack system for indoors with two lightweight 3D Velodyne LiDAR devices and a computer and a modified version for outdoors with two GNSS antennas. The backpack system improved viewing range and achieved an average relative error in translation of less than 5 cm indoors but increases to 11.8 cm outside. Iwaszczuk et al. (2019)'s backpack included a third Velodyne LiDAR, Sony cameras, Casio and GoPro cameras, and a MLS system for smooth transition between indoor and outdoor scenes. Blaser et al. (2021) focused on data collection in forest and urban areas.

1.2 Contributions

We present a mobile mapping backpack system for collecting 3D point clouds of forest vegetation and discuss the advantages and drawbacks of the system's architecture, devices and data collection. Our contributions include:

- defining the requirements for a terrestrial mobile mapping system in forest environment
- testing and comparing two published SLAM algorithms for the use in forests on our backpack
- testing our system in an environment with a forest like vegetation, and comparing our data collection and laser scan quality to terrestrial and airborne laser scanning.
- testing a multi-spectral 10 band camera on a mobile mapping backpack system and discussing the integration and difficulties we encountered while generating a point cloud from the multi-spectral camera. To our knowledge we are the first to include such a camera.

With the extra bands in the multi-spectral camera, we can calculate a vegetation health index using the red and near-infrared bands. Our solution is easy to use and could be used by foresters when they walk through their forest district. Their hands are free and their pace normal when collecting data. The resulting point cloud is directly available to be examined. Our approach allows rapid data collection for databases and inventory as well as being a foundation for further analysis by scientists and foresters. We publish all ROS related software used for this project: `https://git-ce.rwth-aachen.de/fg-fub/DeepForest/dp_ROS`

2. SYSTEMS HARDWARE

This section will first highlight the requirements for the mobile mapping system, followed by a detailed list of implemented sensors and devices in the system.

2.1 Requirements

The mobile mapping system is designed to collect data in a forest environment, hence it must be self-contained. As a result, all devices require enough power to operate for several hours. It must also be possible to evaluate the acquired data on-site in order to determine whether the area needs to be scanned again or if the data quality is enough. Further, it must work without access to GNSS information. Even though the data collection is outside, we find that under the canopy good GNSS positioning is difficult and unreliable. For this reason, the system relies on SLAM to register all individual point clouds during scanning and build a robust point cloud in a relative coordinate system. The system does not need to be water proof, as scanning in the rain or snow is not recommended because the rain drops or snowflakes will cause numerous false points in the point cloud.

We designed the system to be carried as a backpack by a person. We could not use a wheeled system because the terrain is too rough and sometimes muddy. Furthermore, we are interested in crisscrossing standard forest paths. In this environment, a handheld system can also be used. However, we want to connect many different sensors and therefore did not wish to constraint ourselves on a single LiDAR and IMU device. All decisions were based on robustness, rigidity, and weight. A robust carrying system is necessary since the sensors must remain static to each other despite the walking person's movement. Driving close to the point of interest is frequently unrealistic. This requires carrying the backpack to the location of interest. As a result, the backpack must be light and easy to wear for several hours.

2.2 Architecture

The basic design of the backpack is inspired by Blaser et al. (2018)'s backpack. The backpack is carried by Tatonka's Lastenkraxe load carrier, which consists of an aluminium frame welded together with 20 mm and 24 mm wide tubes. An aluminium profile is attached to it, which serves as a support for individual devices. The aluminium strut profiles have a size of 3x3 cm with a 8 mm slot. The backpack weights with devices

Device Type	Company	Dimensions [mm]	Weight [g]	Power Consumption [W @ V]	Powered by
LiDAR	Velodyne	72.7 x 103.3 (H x Diameter)	830	8.0 @ 9.0-18.0	Battery
IMU	Xsens	57 x 42 x 24	55	0.5 @ 4.5-34.0	Computer
IMU	Microstrain	76 x 68.6 x 13.3	48	2.0 @ 5.0-16.0	Computer
Multi-spectral Camera	MicaSense	87 x 123 x 76	508.8	8.0-16.0 @ 4.2-15.8	Power Bank
Computer	Lenovo	329 x 227 x 18	1460	3.8	-
Battery	i-tecc+	180 x 75 x 170	2600	19Ah @ 12,9 V	-
Power Bank	Trust.	28 x 75 x 150	462	20Ah @ 3.7 V	-

Table 1. Specifications of devices installed in the backpack system. Note that there are two IMU listed, but there was always only one built in. W @ V is the power watts at a voltage range of volts.

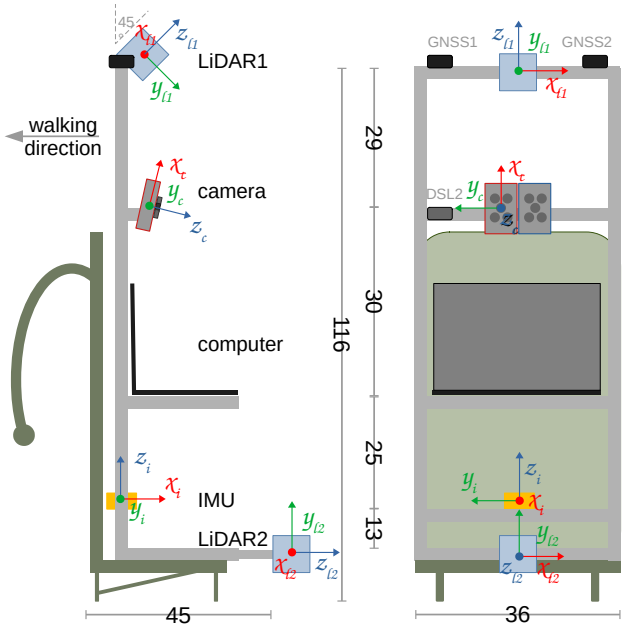

Figure 2. Coordinate systems of the LiDARs (l), IMU (i) and camera (c) before the transformations, and the dimensions of the backpack system (cm). The backpack coordinate system origins at the centre of the IMU, and its x axis is equal to the walking direction.

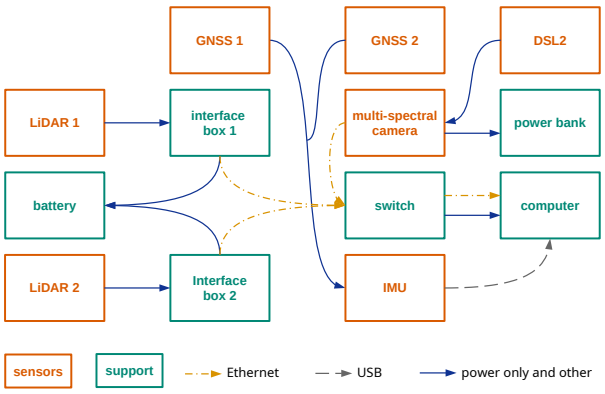

Figure 3. Hardware connectivity between sensors and supportive devices. The arrow ”power only and other” represents cable connections that are either only for power supply or do not belong to Ethernet and USB.

15 kg. Included sensors are laser scanners, a camera, an IMU and GNSS antennas. An overview of the implemented devices with their dimensions, weight, power consumption and power source is listed in Table 1. All hardware components are arranged as shown in Figure 1 and Figure 2 and are connected via cable as illustrated in Figure 3.

LiDAR. The two laser scanners Velodyne VLP-16 Puck Lite have 16 scan lines that rotate. At a distance of 1 m the laser spots have a size of 15.4 mm in horizontal direction and 11.0 mm in vertical direction. At this distance, the gap between the scan lines are approx. 86.2 mm, with a given 0.0859° vertical beam divergence.

IMU. We included the Xsens MTi-700 IMU to support the laser point cloud registration. The orientation accuracy is 0.5° RMS in roll/pitch static and dynamic, and a 1.5° RMS in dynamic yaw. When using the GNSS antenna connected to the IMU, the positional error is 1 m horizontal and 2 m vertical. Later on, we replaced this IMU with the Microstrain Model 3DM-GQ7. This device has an accuracy of 0.05° in roll and pitch. The position accuracy when adding the GNSS information is 1.25 m horizontally, 2 m vertically, and heading is at 0.25°. The corresponding dual antenna includes 184 channels, the global systems GPS, GLONASS, Galileo and BeiDou, and the frequencies L1C/A, L2C, L1OF, L2OF, E1B/C, E5b, B1, B2. Note that both devices are inertial navigation systems (INS) as they combine IMU and GNSS, however for simplicity they will be called IMU in this paper.

Camera. The multi-spectral camera MicaSense RedEdge-MX Dual Camera System is composed of two individual cameras with 5 bands each, and a Downwelling Light Sensor (DSL2). DSL2 is for improving reflectance calibration in cases where ambient light conditions are changing in the middle of a data collection, which happens regularly in forests under the canopy. The camera bands include the following electromagnetic wavelengths (band span). Red camera: blue 475 (32), green 560 (27), red 668 (14), red edge 717 (12) and NIR 842 (57). Blue camera: coastal blue 444 (28), green 531 (14), red 650 (16), red edge 705 (10) and red edge 740 (18). The cameras are triggered simultaneously once per second and save one image per band as a 16-bit TIFF file with a size of 1280 × 960 pixel. WiFi or Ethernet can be used for communication. The individual lenses have a field of view of 47.2° HFOV and a global shutter which is synchronised with all 10 sensors. For simplicity we call the set ”camera”, even though there are two cameras. Our solution includes a customised cable for communicating with the camera. We use a DJI gimble to integrate the DSL2 and provide power. There may be a less complicated setup, but it will require good technical knowledge and tools.

Computer. Our computer, a Lenovo ThinkPad 14s Gen 2, includes AMD Ryzen 7 Pro 6850U / 2.7 GHz CPU, 32 GB of RAM, and an AMD Radeon 680M GPU. For connectivity it supplies Gigabit Ethernet port, two USB 3.2 Gen 1 and two USB-C 3.2 Gen 2. The laptop battery, which is a 4-cell lithium polymer with a 52.5Wh capacity, is also important for powering some devices and limiting the backpack’s usage time.

Power sources. Another power source, besides the computer, is the LiFeEnergy 12V.19, which is a LiFePO4 rechargeable battery. The connectors consists of positive and negative poles. Based on our request, the company Visimind has built power cables especially for the connection between Velodyne LiDARs and the poles on the battery. The camera is powered by a power bank. When connecting the camera directly to the computer as power source results in problems. Because the camera consumes so much power, the computer denied the connection after only a few seconds. This causes the camera to turn off and on every few seconds, resulting in an unreliable method of image collection. Thus, we added an extra power bank for the camera. The power bank was originally planned as a backup for the computer, when a long campaign day was planned.

Switch. Communication from the two LiDARs and the camera to the computer is accomplished via Ethernet. For this, we installed the Switch Flex Mini, including 5 ports. It extends 107.16 × 70.15 × 21.17 mm and weights 150 g. In addition, it has a forwarding rate of 7.44 Mpps, switching capacity of 10 Gbps and is powered by the computer via a USB-C port.

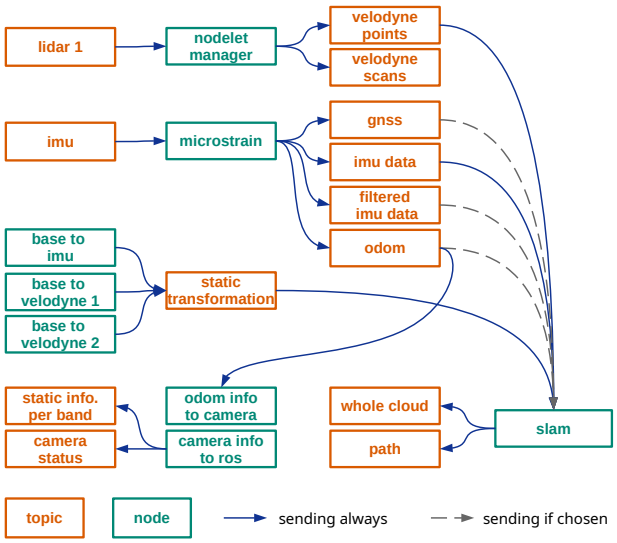

Figure 4. ROS connectivity. The topic LiDAR 2 is identical to LiDAR 1 and was discarded for simplicity.

3. SYSTEMS SOFTWARE

The following sections describe the software architecture, implemented packages, and configurations. An overview of the communication between nodes and sensors is shown simplified in Figure 4. The software is built on ROS. We used published packages by the sensor companies (Velodyne, Xsens, Microstrain) for the conversion and processing into ROS compatible formats. Unfortunately, MicaSense did not support the ROS implementation. Sensor communication is enabled by our self-written scripts, specifically between the MicaSense multispectral camera and the IMU. Thereafter, the target-less calibration LI-Init (Zhu et al., 2022) was used to calibrate the laser scanners and the IMU. Finally, we used the SLAM algorithms FastLIO (Xu et al., 2021b) and StaticMapping (Liu and atinfinity, 2021) with modified parameters.

Our launch file (backpack.launch) sits atop all scripts, connecting the processing and collecting tasks. Underneath is the launch file (backpack_sensors.launch), which starts the connections to the sensors, retrieves the camera information, and sends the IMU's position and timestamp to the camera. SLAM processing could be included in the first launch file, to run live during data collection. However, we noticed after a trial period that this consumes a significant amount of power. As a result, we launch the SLAM node separately and only when we need to inspect the finished point cloud on-site. The topic named static transformation converts the coordinate system of the sensors to a base coordinate system (base_link) and is set based on the device arrangements on the backpack.

The customised script for communicating with the camera within our system is based on the MicaSense general communication guide. Communication is via IP address to the main camera (the red one) and retrieving information such as status, and sending a trigger for continuous image capture. The information from the camera is converted into ROS messages (sensor_msgs/CameraInfo and std_msgs/String) and published in topics, either as general msc_send_status or separately for every band, for instance info_band1. In the opposite direction, information such as position, orientation and timestamp are converted from the IMU (sensor_msgs/Imu for raw data and nav_msgs/Odometry for filtered data) into JSON format and send to the camera. The same procedure is done with the GNSS information (sensor_msgs/NavSatFix) based on the first antenna. If the camera receives this information within one second after capturing, it will be saved in the image metadata.

3.1 Sensor Configurations

We set the Velodynes to save only the strongest signal return. A dual return setting was tried, but it turned out to be ineffective. The data collected was twice as large, but the SLAM algorithm could not process twice as many returns for the same timestamp. Moreover, we chose the strongest return rather than the last return because (1) the laser signal can be disrupted by vegetation and (2) a far-away reflection can be based on noise. Both of these assumptions result in higher point cloud quality when the strongest return is chosen instead of the last return. Further, we set the field of view to 360° and the internal spin rate (RPM) to 600, which converts to 10 frames per second.

The Xsens IMU orientation output was set to quaternion and 100Hz rate to better conform to the ROS guidelines. The inertial data is presented in the form of Rate of Turn and Acceleration. The Microstrain IMU and camera settings were left at their default settings.

3.2 ROS Configurations

the Velodyne configurations or the Xsens package was not changed, except for the IP addresses and frame IDs. We tested the Velodyne package's GNSS extension but decided to only use the GNSS antenna connected to our IMU. In the Microstrain ROS configuration file several parameters for the were set unequal to the default. In addition to changing the frame ID of the published data, we set it to use the ENU frame rather than NED, as well as the computer's timestamp rather than the device's or ROS's. Both the dual antenna GNSS and the GNSS kinematic should be used for auto-heading alignment. We changed the relative position to be published as LLH instead of ECEF.

For a target-less calibrate of the 6DoF rigid transformation and the time offset between one of the 3D LiDAR and the IMU, we used the tool LI-Init Zhu et al. (2022). This involves rotating

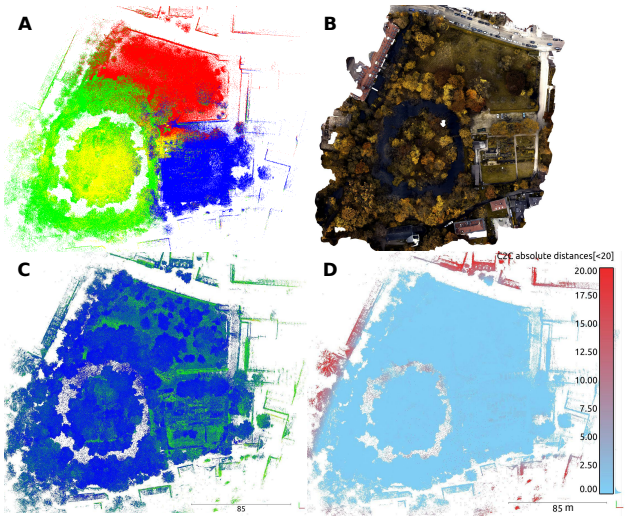

Figure 5. Data collection in monastery garden. (A) The four MLS sets each coloured differently. (B) An orthophoto, based on UAV data. (C) The merged MLS point cloud, coloured in intensity, with blue being the lowest. (D) Cloud to cloud distance error between MLS and ALS point cloud, in meters. For a better visualisation, the reader is advised to view the digital version and zoom in.

the backpack around all axes and moving it in each direction sequentially. As recommended by the authors, we set the filter size surf and map to 0.5 for outdoor environments. The number of iterations was increased from 5 to 100. The rigid transformation from the calibration result is LiDAR1 [-0.02 0.0 0.83 || 3.14 0.785 0.0] and LiDAR2 [-0.37 0.0 -0.15 || -1.57 1.57 -1.57], in the format x y z || yaw pitch roll and given in meters and radians, respectively. The backpack x axis must be directed in the walking direction to be ROS compliant, thus both IMUs are rotated with yaw=3.14 rad. The time lag between LiDAR and IMU, was -0.002 sec for LiDAR1 and -0.009 sec for LiDAR2.

The two SLAM algorithms that have been implemented are FastLIO and StaticMapping. FastLIO does not use GNSS data in either its SLAM optimisation or its final result. Many settings in StaticMapping can be altered; for example, we experimented with various maximal range values. The Velodyne scanner can scan up to 100 m away, but the noise and footprint increase with increasing distance from the light impulse. We started with 70 m, which already gave a good results, but it had a lot of detached points or mismatches in the SLAM result. With 40 m, all of the tree pikes could still be detected and the noise reduced. For example, in the Munich data set, the highest tree is 38 m tall. For the SLAM node, it can be chosen whether to use the raw IMU or the filtered IMU data, if the latter is chosen, the raw data is ignored.

4. EXPERIMENTS AND RESULTS

The survey area is located in Munich, Germany, in a monastery garden (WGS84 LAT 48.14566389652382, LON 11.457112873733656), and covers approximately 21 394 m² (Figure 5B). On the 25th of October 2022, a sunny day with light winds, the tree leaves began to change colour and fall. This area was scanned with TLS and MLS on the same day, and ULS a week earlier. The TLS data was scanned with Leica RTC360. Control points were distributed throughout the area, which were partly a variety of black circle segments and partly two black squares set in a diagonal order and printed on a 210 × 297 mm piece of paper. ALS data was scanned in February 2022 and published by the State Office for Digitisation, Broadband and Surveying, Bavaria, Germany.

The MLS scan was divided into four parts because the area was large and the rosbag files should not be too big to ensure proper post-processing (Figure 5A). In addition, it ensures that should a problem occur, less area must be re-scanned. In Figure 5A, B, and D the white circle represents a water surface. It was scanned first on the island (yellow scan), then on the outer ring (green scan). They were all run through the Fast-LIO algorithm with full range scan distance and then aligned to the ALS data in post-processing. Thereafter the clouds were merged to form one large point cloud, which is portrayed as an intensity scale, with blue being the lowest intensity (Figure 5C). The blue points represent mostly tree crown tops with low intensity.

Point errors can occur in two ways: (1) erroneous point cloud registration can cause objects to be misplaced or visible twice, and (2) point location precision decreases as the laser impulse is reflected further away. To investigate these errors, we compare the registered MLS data to the ALS data, as the TLS data has a strong registration error. Using cloud to cloud absolute distance measurements, from the software CloudCompare, the errors are averaged over all axes. The lower the error from the MLS to the ALS point cloud, the more blue the point is coloured (Figure 5). The small histogram on the right side of the colour scale shows that the error mostly lies near zero. Only the objects that where far away from the sensor, such as high buildings across the street, have a higher error. This emphasises the importance of lowering the maximum range, as the example here was done collected without range reduction. An error is also visible in the vegetation and the water (white ring).

The MLS and ALS data was not captured in the same time period (8 months apart), which is why the vegetation can have grown or slightly moved between the scans. The objects do not seem to occur twice. If we remove the buildings at the far end and the extreme outliers, we get an average error of 27.9 (SD 13.6) cm. Broken down into the three directions: mean error in x direction of 0.4 (SD 3.6) cm, y direction -0.8 (SD 3.4) cm, and z direction 0.6 (SD 6.5) cm. Lastly, when we only focus on the fruit tree meadow (northern part) we receive a mean error in x direction of -0.3 (SD 2.6) cm, y direction -1.7 (SD 3.0) cm, z direction 0.2 (SD 3.6) cm and overall 23.2 (SD 9.2) cm.

TLS data has a registration error, as objects appear twice in the point cloud (Figure 6C). Therefore a comparison should be taken with caution. TLS shows finer details than MLS, visible on the bridge and tree stems (Figure 6D), and therefore a more details representation of the vegetation (Figure 6F).

The registration of the multi-spectral images and the generating of a 3D point cloud was performed with Structure from Motion (SfM) and the software Metashape (version 1.7.6) (Figure 7A). When the camera was set up on the backpack the result was not satisfying (Figure 7A). Nonetheless, the image information is still useful, for example the healthy vegetation shown in red while other objects as well as dead plants are not red (Figure 7B). This red colour represents the NIR information not visible with the human eye. To test the general performance of the camera data, we held the camera parallel to the ground in

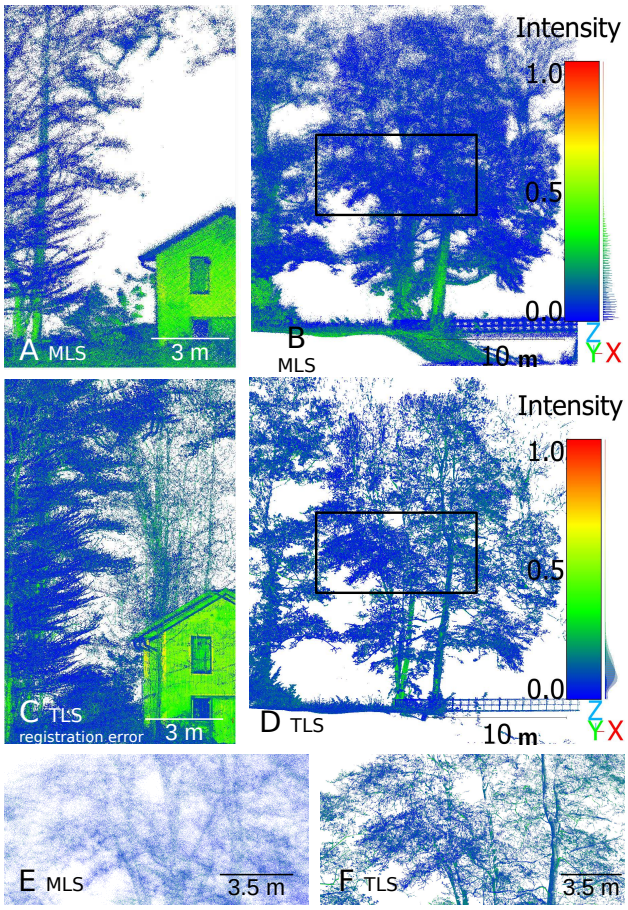

Figure 6. Comparison of MLS and TLS data with registration quality (A,C) and level of detail (B,D-F). MLS full point cloud only from LiDAR1, TLS in (D, F) one scanning point only. The area in the black rectangles (B,D) is enlarged in (E,F).

a height of one meter and moved only on horizontal direction. The result is a 3D reconstruction of the objects and the foliage (Figure 7C).

5. DISCUSSION

5.1 Data collection

It is well known, that MLS needs less time for data collection than TLS. MLS started at each subset of the area and finished after approximately 12 min with the longest run. Most of the time, the team waited roughly an hour for the TLS data collection to be finished. It was also tedious, even though it had a build in relocation estimate, but the tripod had to be repositioned every few meters and the user needed to hide during scans. Nonetheless, the point density is much higher than from the Velodyne VLP16 (Figure 6E and F). The MLS data collection can be done by one user alone and is less dependent on ground roughness or possible stairs. The user can walk at a steady pace. We also compared it to a NavVIS VLX, and it was faster to scan with ours and more comfortable to carry, but the NavVIS VLX had a more detailed and higher quality result.

There are two LiDAR devices installed on the backpack. We observed that the upper one (LiDAR1) returns better or equal results than the lower one during experiments, and particularly during post-processing. We also came to the conclusion that the

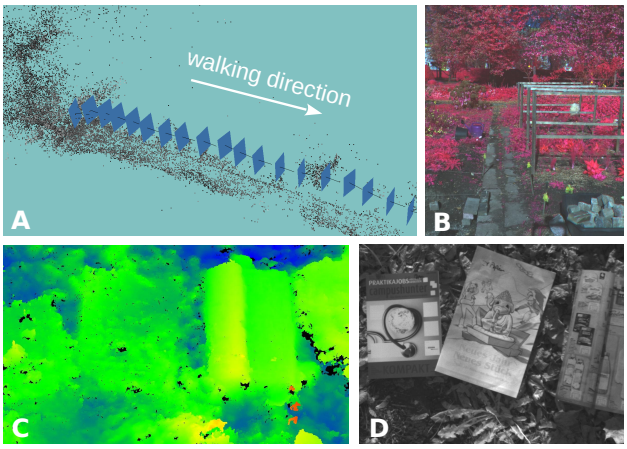

Figure 7. Data from the multi-spectral camera. 3D point cloud with camera attached to the backpack, image locations as blue squares and perpendicular directions as black lines (A), and camera moved 1 m above and parallel to the ground coloured in height, blue is low (C). Image coloured in infrared (NIR, red, green) (B) and image coloured only in NIR (D). Images display the same area as their 3D point cloud, respectively.

upper laser scanner alone can be used to get a good point cloud from the canopy, the ground and the tree stems. Therefore, we recommend including only the upper LiDAR. Besides reducing one LiDAR, we recommend lowering the backpack height. In our experience, this tall construction makes it more difficult to move through a dense forest with low hanging branches. It is unlikely that the person wearing the backpack will block the laser signals, since the laser is mounted at an angle that directs the laser signals steeply upwards. Lastly, the higher point density of a TLS is not necessary to generate a 3D model for foresters to use as a base for their inventory collection, and only takes in more storage capacity and processing.

Changing the IMU from the older Xsens Mti-G-700 to the newer Microstrain has improved the positioning of the backpack. The newer device has a better correction process of the raw data. Unfortunately, the transition from one device to the other, did not go as smoothly as expected. The newer device has more settings, which must be altered to fit into the rest of the system and also satisfy the ROS guidelines.

The camera is initially intended to be mounted on UAVs, which resulted in some difficulties mounting it on a backpack system. The camera is only available with a DJI port or a few cables. However, these cables do not support the included DSL2 and can only communicate via WiFi. An Ethernet connection, on the other hand, is more reliable and faster than a WiFi connection. The company provides instructions for making an Ethernet cable at home for the camera, but the parts required are only available in the United States, or in a set that includes unnecessary items. In addition, the narrow field of view is not suitable for a close range setup. The camera can only cover a small area of the laser scanner point cloud. We do not recommend using this camera for a backpack system as it is difficult to install and connect and the data coverage is small. Connecting the camera with a DJI gimble to a power bank and carrying a laptop with a communication via WiFi could be solution to collect images of forests and other vegetation. This may answer close range questions where multi-spectral data is needed.

5.2 Data Processing

Even though FastLIO succeeds at some situations better than StaticMapping, it lacks the ability to include GNSS information in the SLAM process and the results. Additionally, StaticMapping outputs a path, which FastLIO does not. Furthermore, FastLIO retains more points in the final output, but it adds thick lines (point cluster) to places where the system was unmoved. In open fields, FastLIO performed better in closing the loops. Both SLAM algorithms performed well in the forest settings even without GNSS data. Note, that FastLIO will always produce a point cloud, even if nothing can be correctly matched. StaticMapping indicates throughout the process how many matches it found and of what quality, and if there weren't enough, it won't save a point cloud.

The bad image registration results may be from moving away from objects rather than moving sideways. Thus objects will have a variation in size in each image. In aerial images, the drone or airplane moves in a line parallel to the ground and maintains its flying altitude. Objects appear in the same size in all of the images, making image alignment simpler. There are examples, where such a reconstruction works, however they often use videos instead of images, and our camera can only save one image per second. The experiment when moving parallel to the ground (Figure 7C and D) with a close proximity of the objects to the camera and the relatively wide baseline between the bands in the lens centres, where not the cause of the bad point cloud generation. The camera images alone show useful information (Figure 7B). Not only vegetation shows a high reflectivity in NIR, but also plastic such as plastic boxes, bags or jackets. This can be used to find plastic trash in forests quicker.

6. CONCLUSIONS

The backpack demonstrates its convenience in forest settings. It is easily transportable next to forest paths and rough terrain. Experiments show that two LiDARs are useful for outdoor vegetation tasks, but a single scanner installed at an angle suffices to save money. The system collects less data than TLS, but the level of detail in TLS data is often not necessary. Less storage space is required, and irrelevant object details are not gathered. The point quality was also satisfying. Despite the fact that SLAM is challenged in forest environments, we achieved good results in many field trips to the forest and in the monastery garden with little effort. Both StaticMapping and FastLIO returned good results, but had their difficulties in some environments. For outdoor SLAM, StaticMapping is preferable because it includes GNSS information in its calculations. In cases where GNSS positioning fails, ALS can be used to obtain a good georeference in post-processing. The camera can only cover a small area of the laser scanner point cloud and this camera model is not easy to integrate and images were difficult to align. In the future we will test different positions on the backpack to improve to image alignment and fusion to the point cloud. We suggest to test other camera models. Finally, we want to improve georeferencing in the StaticMapping algorithm.

7. ACKNOWLEDGEMENTS

This study is part of the project "DeepForest: Development of machine learning methods for estimating low forest vegetation from airborne laser point cloud," funded by the Hessian Ministry of Higher Education, Research, Science, and the Arts' LOEWE Exploration program. We thank Sebastian Hunger, Arash Javanmard-Ghareshiran, Jakob Schmidt and Mahmut Tasar for their support during the backpack development and data processing. We also thank Ludwig Hoegner from the University of Applied Sciences Munich as well as the Photogrammetry and Remote Sensing group from the Technical University of Munich for organising the data collection campaign and for sharing their UAV and TLS data.

References

Bettinger, P., Merry, K., Fei, S., Weiskittel, A., Ma, Z., 2023. Usefulness and Need for Digital Technology to Assist Forest Management: Summary of Findings from a Survey of Registered Foresters. *Journal of Forestry*, 121(1), 1–11.

Blaser, S., Cavegn, S., Nebiker, S., 2018. Development of a portable high performance mobile mapping system using the robot operating system. *ISPRS Annals of the Photogrammetry, Remote Sensing and Spatial Information Sciences*, Copernicus GmbH, 13–20.

Blaser, S., Meyer, J., Nebiker, S., 2021. Open urban and forest datasets from a high-performance mobile mapping backpack – a contribution for advancing the creation of digital city twins. *The International Archives of the Photogrammetry, Remote Sensing and Spatial Information Sciences*, Copernicus GmbH, 125–131.

Calders, K., Verbeeck, H., Burt, A., Origo, N., Nightingale, J., Malhi, Y., Wilkes, P., Raumonen, P., Bunce, R. G. H., Disney, M., 2022. Laser scanning reveals potential underestimation of biomass carbon in temperate forest. *Ecological Solutions and Evidence*, 3(4), e12197.

Campos, M., Litkey, P., Wang, Y., Chen, Y., Hyyti, H., Hyyppä, J., Puttonen, E., 2020. A Terrestrial Laser Scanning Measurement Station to Monitor Long-Term Structural Dynamics in a Boreal Forest. *The International Archives of the Photogrammetry, Remote Sensing and Spatial Information Sciences*, XLIII-B1-2020, 27–31.

Elsherif, A., Gaulton, R., Mills, J. P., 2019. The Potential of Dual-Wavelength Terrestrial Laser Scanning in 3D Canopy Fuel Moisture Content Mapping. *The International Archives of the Photogrammetry, Remote Sensing and Spatial Information Sciences*, XLII-2/W13, 975–979.

Gallagher, M. R., Maxwell, A. E., Guillén, L. A., Everland, A., Loudermilk, E. L., Skowronski, N. S., 2021. Estimation of Plot-Level Burn Severity Using Terrestrial Laser Scanning. *Remote Sensing*, 13(20), 4168.

Guo, Q., Su, Y., Hu, T., Guan, H., Jin, S., Zhang, J., Zhao, X., Xu, K., Wei, D., Kelly, M., Coops, N. C., 2021. Lidar Boosts 3D Ecological Observations and Modelings: A Review and Perspective. *IEEE Geoscience and Remote Sensing Magazine*, 9(1), 232–257.

Heinzel, J., Ginzler, C., 2019. A Single-Tree Processing Framework Using Terrestrial Laser Scanning Data for Detecting Forest Regeneration. *Remote Sensing*, 11(1), 60.

Huo, L., Lindberg, E., Holmgren, J., 2022. Towards low vegetation identification: A new method for tree crown segmentation from LiDAR data based on a symmetrical structure detection algorithm (SSD). *Remote Sensing of Environment*, 270, 112857.

Iwaszczuk, D., Goebel, M., Du, Y., Schmidt, J., Weinmann, M., 2023. Potential of Mobile Mapping to Create Digital Twins of Forests. *The International Archives of the Photogrammetry, Remote Sensing and Spatial Information Sciences*, XLVIII-1/W1-2023, 199–206. https://isprs-archives.copernicus.org/articles/XLVIII-1-W1-2023/199/2023/.

Iwaszczuk, D., Koppanyi, Z., Pfrang, J., Toth, C., 2019. Evaluation of a Mobile Multi-Sensor System for Seamless Outdoor and Indoor Mapping. *Int. Arch. Photogramm. Remote Sens. Spatial Inf. Sci.*, XLII-1/W2, 31–35.

Javanmard-Gh., A., Iwaszczuk, D., Roth, S., 2021. DeepLIO: Deep Lidar Inertial Sensor Fusion For Odometry Estimation. *ISPRS Annals of the Photogrammetry, Remote Sensing and Spatial Information Sciences*, V-1-2021, 47–54. https://isprs-annals.copernicus.org/articles/V-1-2021/47/2021/.

Jeronimo, S. M. A., van Kane, R., Churchill, D. J., McGaughey, R. J., Franklin, J. F., 2018. Applying LiDAR Individual Tree Detection to Management of Structurally Diverse Forest Landscapes. *Journal of Forestry*, 116(4), 336–346.

Kohlbrecher, S., Meyer, J., von Stryk, O., Klingauf, U., 2011. A flexible and scalable slam system with full 3d motion estimation. *Proc. IEEE International Symposium on Safety, Security and Rescue Robotics (SSRR)*, IEEE.

Kukko, A., Kaijaluoto, R., Kaartinen, H., Lehtola, V. V., Jaakkola, A., Hyyppä, J., 2017. Graph SLAM correction for single scanner MLS forest data under boreal forest canopy. *ISPRS Journal of Photogrammetry and Remote Sensing*, 132, 199–209.

Lauterbach, H., Borrmann, D., Heß, R., Eck, D., Schilling, K., Nüchter, A., 2015. Evaluation of a Backpack-Mounted 3D Mobile Scanning System. *Remote Sensing*, 7(10), 13753–13781.

Liang, X., Hyyppä, J., Kaartinen, H., Lehtomäki, M., Pyörälä, J., Pfeifer, N., Holopainen, M., Brolly, G., Francesco, P., Hackenberg, J., Huang, H., Jo, H.-W., Katoh, M., Liu, L., Mokroš, M., Morel, J., Olofsson, K., Poveda-Lopez, J., Trochta, J., Di Wang, Wang, J., Xi, Z., Yang, B., Zheng, G., Kankare, V., Luoma, V., Yu, X., Chen, L., Vastaranta, M., Saarinen, N., Wang, Y., 2018. International benchmarking of terrestrial laser scanning approaches for forest inventories. *ISPRS Journal of Photogrammetry and Remote Sensing*, 144, 137–179.

Liang, X., Kankare, V., Hyyppä, J., Wang, Y., Kukko, A., Haggrén, H., Yu, X., Kaartinen, H., Jaakkola, A., Guan, F., Holopainen, M., Vastaranta, M., 2016. Terrestrial laser scanning in forest inventories. *ISPRS Journal of Photogrammetry and Remote Sensing*, 115, 63–77.

Liang, X., Kukko, A., Balenovic, I., Ninni, S., Junttila, S., Kankare, V., Holopainen, M., Martin, M., Surovy, P., Kaartinen, H., Luka, J., Honkavaara, E., Nasi, R., Jingbin, L., Hollaus, M., Tian, J., Yu, X., Jie, P., Shangshu, C., Virtanen, J.-P., Wang, Y., Hyyppa, J., 2022. Close-Range Remote Sensing of Forests: The State of the Art, Challenges, and Opportunities for Systems and Data Acquisitions. *IEEE Geoscience and Remote Sensing Magazine*, 2–41.

Liu, E., atinfinity, 2021. Edwardliuyc/staticmapping.

Pohjavirta, O., Liang, X., Wang, Y., Kukko, A., Pyörälä, J., Hyyppä, E., Yu, X., Kaartinen, H., Hyyppä, J., 2022. Automated registration of wide-baseline point clouds in forests using discrete overlap search. *Forest Ecosystems*, 100080.

Shan, T., Englot, B., Meyers, D., Wang, W., Ratti, C., Rus, D., 2020. Lio-sam: Tightly-coupled lidar inertial odometry via smoothing and mapping. *2020 IEEE/RSJ International Conference on Intelligent Robots and Systems (IROS)*, IEEE, 5135–5142.

Shao, J., Zhang, W., Mellado, N., Wang, N., Jin, S., Cai, S., Luo, L., Lejemble, T., Yan, G., 2020. SLAM-aided forest plot mapping combining terrestrial and mobile laser scanning. *ISPRS Journal of Photogrammetry and Remote Sensing*, 163, 214–230.

Stereńczak, K., Kraszewski, B., Mielcarek, M., Piasecka, Ż., Lisiewicz, M., Heurich, M., 2020. Mapping individual trees with airborne laser scanning data in an European lowland forest using a self-calibration algorithm. *International Journal of Applied Earth Observation and Geoinformation*, 93, 102191.

Talkner, U., Paar, U., Klinck, C., Bialozyt, R., 2022. *Forest Environmental Monitoring and Integrated Climate Protection Plan Hesse 2025*. Zenodo.

Velas, M., Spanel, M., Sleziak, T., Habrovec, J., Herout, A., 2019. Indoor and Outdoor Backpack Mapping with Calibrated Pair of Velodyne LiDARs. *Sensors (Basel, Switzerland)*, 19(18).

Wallace, L., Hally, B., Hillman, S., Jones, S. D., Reinke, K., 2020. Terrestrial Image-Based Point Clouds for Mapping Near-Ground Vegetation Structure: Potential and Limitations. *Fire*, 3(4), 59.

Wang, H., Wang, C., Chen, C.-L., Xie, L., 2021. F-LOAM: Fast LiDAR Odometry And Mapping. 4390–4396.

Xu, H., Wang, C. C., Shen, X., Zlatanova, S., 2021a. 3D Tree Reconstruction in Support of Urban Microclimate Simulation: A Comprehensive Literature Review. *Buildings*, 11(9), 417.

Xu, W., Cai, Y., He, D., Lin, J., Zhang, F., 2021b. Fast-lio2: Fast direct lidar-inertial odometry.

Xu, X., Zhang, L., Yang, J., Cao, C., Wang, W., Ran, Y., Tan, Z., Luo, M., 2022. A Review of Multi-Sensor Fusion SLAM Systems Based on 3D LIDAR. *Remote Sensing*, 14(12), 2835.

Zhang, J., Singh, S., 2014. Loam: Lidar odometry and mapping in real-time. *Robotics: Science and Systems X*, Robotics: Science and Systems Foundation.

Zhu, F., Ren, Y., Zhang, F., 2022. Robust real-time lidar-inertial initialization. *2022 IEEE/RSJ International Conference on Intelligent Robots and Systems (IROS)*, IEEE, 3948–3955.

Zong, X., Wang, T., Skidmore, A. K., Heurich, M., 2021. Estimating fine-scale visibility in a temperate forest landscape using airborne laser scanning. *International Journal of Applied Earth Observation and Geoinformation*, 103, 102478.